Published in final edited form as:
*Am J Physiol Heart Circ Physiol*. 2008 April ; 294(4): H1597–H1608.

# Modulation of the late sodium current by $Ca^{2+}$, calmodulin, and CaMKII in normal and failing dog cardiomyocytes: similarities and differences

**Victor A. Maltsev**, **Vitaliy Reznikov**, **Nidas A. Undrovinas**, **Hani N. Sabbah**, and **Albertas Undrovinas**
*Department of Internal Medicine, Henry Ford Hospital, Detroit, Michigan*

## Abstract

Augmented and slowed late $Na^+$ current ($I_{NaL}$) was implicated in action potential duration variability, early afterdepolarizations, and abnormal $Ca^{2+}$ handling in human and canine failing myocardium **Objective** was to study $I_{NaL}$ modulation by cytosolic $Ca^{2+}$ ($[Ca^{2+}]_i$) in normal and failing ventricular myocytes.

**Methods—**Chronic heart failure was produced in 10 dogs by multiple sequential coronary artery microembolizations, 6 normal dogs served as a control. $I_{NaL}$ fine structure was measured by whole-cell patch-clamp in ventricular myocytes and approximated by a sum of fast and slow exponentials produced by burst and late scattered modes of $Na^+$ channel gating, respectively.

**Results—**$I_{NaL}$ greatly enhanced as $[Ca^{2+}]_i$ increased from "$Ca^{2+}$ free" to 1μM: its maximum density increased, decay of both exponentials slowed, and steady-state-inactivation curve (SSI) shifted towards more positive potentials. Testing inhibition of CaMKII and CaM revealed similarities and differences of $I_{NaL}$ modulation in failing vs. normal myocytes. Similarities: 1) CaMKII slows $I_{NaL}$ decay and decreases the amplitude of fast exponential; 2) $Ca^{2+}$shifts SSI rightward. Differences: 1) slowing $I_{NaL}$ by CaMKII is greater; 2) CaM shifts SSI leftward; 3) $Ca^{2+}$ increases the amplitude of slow exponential.

**Conclusions—**$Ca^{2+}$/CaM/CaMKII signaling increases $I_{NaL}$ and $Na^+$ influx in both normal and failing myocytes by slowing inactivation kinetics and shifting SSI. This $Na^+$ influx provides a novel $Ca^{2+}$ positive feedback mechanism (via $Na^+/Ca^{2+}$exchanger), enhancing contractions at higher beating rates, but worsening cardiomyocytes contractile and electrical performance in conditions of poor $Ca^{2+}$ handling in heart failure.

### Keywords

heart failure; late $Na^+$ current; calcium; arrhythmia

## 1. Introduction

Augmented and slowed late $Na^+$ current ($I_{NaL}$) in heart failure (HF) (21,46) contributes to action potential (AP) duration variability and development of early afterdepolarizations (EADs) in human and dog ventricular cardiomyocytes (VCs) isolated from failing hearts (16,

Address for correspondence: Albertas Undrovinas, Ph.D., Henry Ford Hospital, Cardiovascular Research, Education & Research Bldg. Room 4015, 2799 West Grand Boulevard, Detroit, MI 48202-2689, Phone: (313)-916-1321, Fax: (313)-916-3001, E-mail: aundrov1@hfhs.org.
Current address of Victor A. Maltsev is Gerontology Research Center, National Institute on Aging, NIH, 5600 Nathan Shock Drive, Baltimore, Maryland 21224, USA

**Disclosures** There are no disclosures

21,46). Interestingly, the amount of $Na^+$ carried by large but short (a few ms) transient $Na^+$ current ($I_{NaT}$) is almost equal to that carried by a much smaller but much longer $I_{NaL}$ (hundreds of ms) (21,23). Since $I_{NaT}$ is reportedly decreased (19,54) but $I_{NaL}$ is increased in HF, the latter likely provides an important contribution to the increase in intracellular $Na^+$ ($[Na^+]_i$) and to a higher cell $Ca^{2+}$ load in HF (26). Because of its pathophysiological significance, $I_{NaL}$ recently emerged as a plausible target for cardioprotection therapies (reviews (8,26))

HF-related mechanisms leading to the $I_{NaL}$ augmentation and slower decay are not clear. All previous comparisons of $I_{NaL}$ in normal and failing hearts were performed at low intracellular $Ca^{2+}$ in the presence of strong $Ca^{2+}$ buffers, thus only $Ca^{2+}$-independent changes have been compared so far. Taking into account that $Ca^{2+}$ handling in HF is altered (see review (6), an intriguing question is then whether $Ca^{2+}$ provides any modulatory feedback mechanism to $I_{NaL}$ in HF.

The present study tested if intracellular $Ca^{2+}$ modulates $I_{NaL}$ in VCs and if this modulation is different in normal and failing hearts. For this purpose we employed an established model of canine chronic heart failure produced by the multiple sequential coronary artery microembolizations (34). This model produces array of morphological and functional changes similar to that for humans. In order to get a mechanistic insight to $I_{NaL}$ modulation by $Ca^{2+}$, we tested how signaling via $Ca^{2+}$/calmodulin (CaM)/$Ca^{2+}$-dependent CaM-kinase II (CaMKII) affects the whole-cell $I_{NaL}$ in patch-clamped VCs isolated from normal and failing dog hearts. We found that while the intracellular $Ca^{2+}$ signaling enhances $I_{NaL}$ in both normal and failing VCs, its modulation range is larger in HF. This result indicates that previous evaluations of functional importance of $I_{NaL}$ in normal and especially in failing hearts might be underestimated because they were based on $Ca^{2+}$ independent $I_{NaL}$ function. Preliminary data of this study have been reported as an abstract (18).

## 2. Materials and Methods

### 2.1. HF model and myocyte isolation

The study conforms to the Guidelines for Care and Use of Laboratory Animals published by the US National Institutes of Health and was approved by the Animal Care and Use Committee (IACUC) of the Henry Ford Health System. Chronic heart failure that is similar by vast array of functional and pathophysiological parameters (33) to that in humans was produced in 10 dogs by multiple sequential coronary artery microsphere embolizations as previously described (34). Six normal dogs served as a control. At the time of harvesting the heart (~3 months after last embolization), left ventricular (LV) ejection fraction was approximately ~25%. Cardiomyocytes were enzymatically isolated from the apical LV mid-myocardial slices as previously reported (16). The yield of viable rod-shaped, $Ca^{2+}$-tolerant VCs varied from 40 to 70%.

### 2.2. Patch clamp technique and data analysis

$I_{NaL}$ was measured using a whole-cell patch-clamp technique (16,46). $I_{NaL}$ was assessed by 2s membrane depolarizations to various potentials from a holding potential of -130 mV applied with a stimulation frequency of 0.2 Hz, and presented in terms of the current density (pA/pF), i.e. $I_{NaL}$ = (whole cell $I_{NaL}$) / $C_m$, where $C_m$ is cell electric capacitance that was measured by a voltage ramp (19) in each cell. The composition of bath (B) and pipette (P) solution is shown in Table 1. Experiments were performed at room temperature (22-24°C). All measurements were made 8-25 min after the membrane rupture to complete cell dialysis with intracellular recording solutions (24,28,31). In previous studies peptides or small proteins such as protein kinase catalytic subunits (14) can quickly (within 5 minutes) reach their targets in adult ventricular myocytes during a whole cell dialysis via patch pipette.

The fine structure of $I_{NaL}$ time course has been approximated by a double exponential fit to $I_{NaL}$ decay starting at 40 ms after the onset of depolarization to −30 mV as previously suggested (23):

$$f(t)=I_{40}\cdot\{k_1\cdot exp(-t/\tau_1)+k_2\cdot exp(-t/\tau_2)\} \quad (1)$$

where $\tau_1$ and $\tau_2$ are the time constants, $I_{40}$ is $I_{NaL}$ instant value 40 ms after membrane depolarization, $k_1$ and $k_2$ are the contributions of each exponents ($k_1 + k_2 = 1$), respectively. 5-15 experimental traces were averaged to improve the quality of analysis.

The steady-state inactivation (SSI) was evaluated by a double-pulse protocol with 2s-duration pre-pulses (Vp) ranging from −130 mV to -40 mV followed by a testing pulse to -30 mV. INa amplitudes were normalized to that measured at Vp= -130 mV and the data points were fitted to a Boltzmann function A(Vp):

$$A(V_p) = 1/(1 + \exp((V_{\frac{1}{2}A} - V_p)/k_A)) \quad (2)$$

The steady-state activation (SSA) parameters were determined from the current-voltage relationships by fitting data points of the normalized current with the function (19):

$$I_{Na}(V_t) = G_{max} \cdot (V_r - V_t)/\{1 + \exp[(V_{\frac{1}{2}G} - V_t)/k_G]\} \quad (3)$$

Where $G_{max}$ is a normalized maximum $Na^+$ conductance, $V_r$ is a reversal potential; $V_{½G}$, and $k_G$ are the midpoint and the slope of the respective Boltzmann function underlying the steady-state $Na^+$ channel activation. The $I_{NaL}$ data points in the current-voltage relationships were measured as the averaged current density within 200-220 ms after depolarization onset (vertical bar in Figs.1A, B, 3A, B, 5A, B).

### 2.3. Statistical Analysis

Multiple comparisons between treatment groups were made using one-way analysis of variance (ANOVA) followed by Bonferroni's post hoc test. Data are reported as mean±SEM. The significance of SSA or SSI changes were evaluated using F-test (StatMost, DataMost Corp., Salt Lake City, UT) for tabulated values predicted by the model (Eqs.2, 3) at a confidence level of 0.95. Differences for both experimental data and model predictions were considered statistically significant for $P<0.05$.

### 2.4 Chemicals

Collagenase type II (291 U/mg) was from Worthington (Freehold, NJ). CaM, CaM binding domain, peptide 290-309, and CaMKII inhibitor KN93 and its inactive analog KN92 were purchased from Calbiochem (Darmstadt, Germany). All other chemicals and enzymes were purchased from Sigma (St. Louis, MO).

## 3. Results

### 3.1. Elevated intracellular $Ca^{2+}$ slows decay of $I_{NaL}$, increases density, and shifts SSI in both normal and failing hearts

First we compared $I_{NaL}$ decay time course, density, SSA and SSI at low (depicted as "0$Ca^{2+}$") and high ("1μM $Ca^{2+}$") intra-pipette $[Ca^{2+}]_i$ (solutions composition are depicted in Table 1). Two intracellular $Ca^{2+}$ buffering agents were tested; EGTA and BAPTA ($P_1$ and $P_2$ in Table 1). Although BAPTA provides more stringent $Ca^{2+}$ buffering and more rapid $Ca^{2+}$ binding kinetics (50), no difference was found for $I_{NaL}$ decay kinetics, density, or SSI

when using these buffers (not shown). Accordingly, "0$Ca^{2+}$" refers further to EGTA buffer. Elevated $[Ca^{2+}]_i$ substantially increased amplitude and slowed inactivation of $I_{NaL}$ in both normal and failing hearts (Fig.1). Both $\tau_1$ and $\tau_2$ significantly increased in the elevated $Ca^{2+}$ (Fig.1C, D). For example, at -30 mV (maximum $I_{NaL}$) their average values in "0$Ca^{2+}$ "and " 1μM $Ca^{2+}$" in normal hearts were as follows: $\tau_1$ = 31.3 ±0.7; $\tau_2$=417.7±9.1 ms, n= 27 VCs (4 hearts) *vs.* $\tau_1$ = 48.6 ±2.1; $\tau_2$=487±18 ms, n= 11(2) (p<0.005, ANOVA), respectively. For HF: $\tau_1$= 35.2±1.9; $\tau_2$=505.7±19.2 ms, n= 12 (4) *vs.* $\tau_1$= 57.4 ±3.7; $\tau_2$=625.6±42 ms, n= 28 (8) (P<0.005), respectively. Interestingly, both time constants were significantly different at the same $[Ca^{2+}]_i$ when compared normal *vs*. failing VCs. However, relative contribution of these exponents remained almost unchanged (normal heart, $k_2$= 0.43±0.02 *vs.* 0.46±0.05, 0$Ca^{2+}$ *vs.* 1μM $Ca^2$; HF, $k_2$= 0.41±0.05 *vs.* 0.43±0.04, respectively, NS). Elevated $[Ca^{2+}]_i$ significantly increased $I_{NaL}$ density (Table 2) in a wide range of voltages, including potentials of the AP plateau in both normal and failing hearts (Fig. 2A, B). Another noticeable effect of the $Ca^{2+}$ elevation was a shift (~5.8 and ~4.4 mV for normal and failing hearts, respectively) of the SSI mid-potential towards positive potentials (Fig.2 C, D, Table 3) without changes in the SSA mid-potential (Fig. 2A, B)

### 3.2. Infusion of CaM does not affect $I_{NaL}$

To test if intrinsic intracellular amount of CaM can limit effects of elevated $[Ca^{2+}]_i$ on $I_{NaL}$, we infused additional CaM molecules in the presence of 1μM $[Ca^{2+}]_i$. The $I_{NaL}$ decay, density and SSI (not shown) parameters were not significantly affected by the intracellular infusion of CaM into the cells *via* the patch pipette. These data indicated that $[CaM]_i$ either is not involved in $Ca^{2+}$ modulation of $I_{NaL}$ or remains high enough during the whole cell recordings to mediate $Na^+$ channel modulation by $Ca^{2+}$. Thus, the absence of any effect of CaM infusion served as a control for our further experiments with peptide P290-309, which were designed to clarify the role of CaM in $I_{NaL}$ modulation by testing effects of CaM inhibition (see below).

### 3.3. Effects of a CaMKII inhibitor KN93

In the presence of high $[Ca^{2+}]_i$, CaMKII inhibition by KN93 caused two major effects (see examples of recordings in Fig.3 A, B): 1) $I_{NaL}$ decay acceleration (both fast and slow components of $I_{NaL}$) in both normal and failing hearts blunting the difference in terms of $I_{NaL}$ inactivation kinetics between these two specimens (Figs.3C,D); 2) significant $I_{NaL}$ density reduction observed at various levels of testing voltages within the range of action potential plateau (as the whole-cell conductance decreased) in failing but not in normal hearts (Fig.4 A, B, Table 2). The $V_{1/2}$ of the SSA in both normal and failing hearts changed insignificantly. There was no significant effect on SSI by KN93 in either normal or failing hearts compared with the augmented $[Ca^{2+}]_i$ (Fig. 4 C, D, Table 3).

To provide a control for the substantial KN93 effect on $I_{NaL}$ kinetics, we also tested the effect of KN92 (an inactive analog of KN93): In the presence of 1 μM $[Ca^{2+}]_i$ and 10 μM KN92 the $I_{NaL}$ kinetics and SSA remained unchanged (n=16(4) HF, not shown)). However, we did not compare effects of KN93 and KN92 on SSI due to two reasons 1) CaMKII blockade by KN93 had no effect on SSI, 2) well-known nonspecific effects of KN92 on SSI (9).

### 3.4. Effects of interference to $Ca^{2+}$-dependent CaM binding

Infusion of P290-309, a potent CaM antagonist, in the presence of high $[Ca^{2+}]_i$ caused two effects described above for KN93, i.e. $I_{NaL}$ decay acceleration and density decrease (Fig.5, Table 2); and this was expected because inhibition of CaM is a less specific intervention that includes CaMKII inhibition (CaMKII function is by definition is CaM dependent). However, a specific effect of CaM inhibition that was not observed under KN93 was a significant shift of SSI curve towards positive potentials in failing but not in normal hearts (Fig.6 C, D, Table 3).

### 3.5. Interpretation of experimental data in terms of $Ca^{2+}$ modulation of $I_{NaL}$ gating modes and $I_{NaL}$-mediated $Na^+$ influx

While the experimental data (Figs. 3-6) of various interventions to $Ca^{2+}$ regulatory pathways provide mechanistic insights into $I_{NaL}$ regulation by those pathways (biochemical insights), additional analysis is required to evaluate numerically modulation by those pathways of various $I_{NaL}$ gating modes (23,45) (biophysical insights) and of $I_{NaL}$ mediated $Na^+$ influx into the cells (physiological insights). In our experiments the $I_{NaL}$ density was measured 200 ms after membrane depolarization, and the $I_{NaL}$ kinetics were evaluated starting from 40 ms. Thus, the observed changes in the density can be due to either $I_{NaL}$ slowing or a decrease in the number of $Na^+$ channels operating in the late gating modes. To address this question, the fine structure of the entire $I_{NaL}$ time course has been further analyzed based on $I_{NaL}$ approximation by a double exponential function in Eq.2, which allows an easy interpretation of the whole cell data in terms of gating modes of late $Na^+$ channel openings. Contrary to a prediction of a non-inactivating $I_{NaL}$ by a non-unique model of $Na^+$ channel gating (11), patch clamp studies in human ventricular myocytes showed that both the burst mode (BM) and the late scattered mode (LSM) openings do inactivate! (29,45). A recent unique numerical model (23) of $Na^+$ channel gating based on the single channel data of late openings describes the entire $I_{NaL}$ time course as a sum of two exponentials: BM generates the fast, exponentially decaying $I_{NaL}$ component ($I_{BM}$), whereas LSM openings generate a relatively slow $I_{NaL}$ decaying component ($I_{LSM}$):

$$I_{BM}(t) = I_{40} \cdot k_1 * e^{-(t-40ms)/\tau_1} \tag{4}$$

$$I_{LSM}(t) = I_{40} \cdot k_2 * e^{-(t-40ms)/\tau_2} \tag{5}$$

Where $I_{40}$, $k_1$, $k_2$, $\tau_1$, and $\tau_2$ are from Eq.1. Using the above approximations, we evaluated the following important parameters: amplitudes $I_{BM}(0)$ and $I_{LSM}(0)$ and integrals $Q_{BM}$ and $Q_{LSM}$ of the fast and slow $I_{NaL}$ components, respectively:

$$Q_{BM} = \int_0^{2000\,ms} I_{BM}(t)dt \tag{6}$$

$$Q_{LSM} = \int_0^{2000\,ms} I_{LSM}(t)dt \tag{7}$$

The amplitudes thus reflect the total number of channels in respective gating modes and the integrals reflect the respective $Na^+$ influxes transferred by each mode. Since we found a complex modulation of SSI by $Ca^{2+}$ and CaM, we also evaluated the total integral for INaL elicited from a physiological resting potential of $V_{rest}$=-80 mV:

$$Q_{tot} = A(-80) \cdot (Q_{BM} + Q_{LSM}) \tag{8}$$

where A(-80) is $Na^+$ channel steady-state availability at -80 mV calculated using Eq.2. The results of the analysis are summarized in Table 4 and can be interpreted for each modulation pathway as follows:

CaMKII slows decay kinetics of both BM and LSM openings with the effect being greater in failing VCs, resulting in a substantially larger regulation range of $Q_{LSM}$ by CaMKII in the failing cells, 56.8% vs. 35% (CaMKII modulates $I_{LSM}(0)$, i.e. the number of LSM channels, insignificantly). At the same time, CaMKII substantially decreases $I_{BM}(0)$, i.e. the number of BM channels, with $Q_{BM}$ remaining almost unchanged in both normal and failing cells.

CaM produces no additional modulatory effects on the fine structure of $I_{NaL}$ rather than those described above for CaMKII modulation. Hence, the only major and specific effect of CaM on $I_{NaL}$ is the negative SSI shift in the failing cells.

$Ca^{2+}$itself, independently of CaM, increases $I_{LSM}(0)$ (reflecting the number of LSM channels) by ~30.7% in failing cells but produces no effect on this parameter in normal cells. $Ca^{2+}$ also (independently of CaM) shifts SSI to negative potentials. The combined effect of this shift and $I_{LSM}(0)$ increase on $Q_{tot}$ was substantially larger in the failing cells vs. normal cells (150% vs. 61.6%). Interestingly, that CaMKII contribution in $Q_{tot}$ modulation is minor (only ~21%) in the failing cells.

Net $Ca^{2+}$effect on $I_{NaL}$ and its integral is strong in both normal and failing VCs (Fig.7). The absolute modulation range of $I_{NaL}$ is larger in failing cells, with the difference being greater at the beginning of depolarization (shaded area in Fig.7C). The relative instant increase of $I_{NaL}$ produced by $Ca^{2+}$ was larger in failing cells; in both cell types it exhibits an N-like shape with a local maximum at ~120 ms (Fig.7D). CaMKII-mediated slowing of LSM decay and rightward shift of SSI by $Ca^{2+}$ (CaM-independent) turns out to be the major contributors to the $I_{NaL}$ integral change (Fig.7 E-G, Table 4). In HF VCs, while $Ca^{2+}$ increases the number of LSM channels and shifts SSI to more positive voltages, these effects are offset by CaM-induced negative SSI shift, so that the net $Ca^{2+}$- induced increase of $Q_{tot}$ is only moderately higher in HF (135% vs. 101%, respectively, Table 4, see also shaded area in Fig.7G "HF-NORM")

## 4. Discussion

The present study has demonstrated that $I_{NaL}$ in ventricular myocytes of normal and failing dog hearts is strongly enhanced by intracellular $Ca^{2+}$ and this modulation is linked to complex $Ca^{2+}$/CaM/CaMKII signaling (summarized in Table 4 and schematically illustrated in Fig.8). We identified $Ca^{2+}$-dependent modulation mechanisms, which are common and different in normal and failing cells. The common mechanisms include 1) CaMKII slows the $I_{NaL}$ decay kinetics and decreases the amplitude of the fast/bursts $I_{NaL}$ component; 2) direct $Ca^{2+}$ binding shifts SSI curve to more positive potentials. $I_{NaL}$ modulation in failing VCs differs from that in normal cells: 1) slowing of both $I_{NaL}$ components $I_{NaL}$ by CaMKII is greater; 2) $Ca^{2+}$ shifts SSI to more positive voltages; 3) CaM shifts SSI curve to negative potentials; 4) $Ca^{2+}$ increases the amplitude of $I_{NaL}$ slow/LSM component.

### 4.1 Molecular mechanisms of $I_{NaL}$ modulation by $Ca^{2+}$-CaM-CaMKII pathways

Previous studies of $Na^+$ channels have established several pathways for $Na^+$ channel modulation by intracellular $Ca^{2+}$: 1) direct binding of $Ca^{2+}$ ions to $Ca^{2+}$ binding EF-hand motif found in $Na_v1.5$ C-terminus (50), 2) direct CaM binding to IQ motif of $Na_v1.5$ C-terminus (39), 3) activation CaMKII resulting in phosphoryllation of the channel protein (9,49). $Ca^{2+}$ modulation of $Na^+$ channels is a rather complex phenomenon and continues to be a matter of debate (see review (1)) especially when heterologous expression systems and native myocytes are compared. Moreover, conclusions of aforementioned studies are mainly based on recordings of the transient $Na^+$ current that may or may not be relevant to $I_{NaL}$ modulation.

All three above molecular mechanisms can be potentially involved in the effects of complex $Ca^{2+}$/CaM/CaMKII modulation of $I_{NaL}$ characteristics found in the present study (Table 4, Fig. 8). More specifically, we found that late $Na^+$ channel gating is regulated by CaMKII (Fig. 3) in both normal (in line with (49)) and failing hearts, and that $Ca^{2+}$ shifts SSI towards positive potentials (Fig1 C, D) (in line with (50)). The latter effect is likely independent of CaM and CaMKII in normal myocytes because inhibition of either CaM or CaMKII has no effect on SSI (Fig. 6C).

However, specifically in failing cells CaM (independently of CaMKII) offsets, at least in part, the SSI shift associated with the major CaM-independent effect. The negative shift of SSI by CaM-dependent regulation is in line with Tan et al. (39). However, Wagner et al. (49) reported an opposite effect (compared with (50) and our study) of $[Ca^{2+}]_i$ elevation on SSI in rabbit and rat cardiomyocytes, including those in which CaMKII$\delta_C$ was over-expressed. The difference in results could be due to a) different cell types, e.g. tsA201 (50) cells vs. cardiomyocytes; b) perturbation of $Ca^{2+}$ signaling by an over-expression of the signaling proteins; c) different currents used to assess SSI i.e. $I_{NaT}$ or $I_{NaL}$ (our study); d) different recording conditions, e.g. 10 mM (49) vs.140 mM. In fact, occupancy of the $Na^+$ channel pore by the permeant ion substantially affects slow inactivation of the channel (3).

### 4.2. Why is $Ca^{2+}$ modulation of $I_{NaL}$ different in heart failure?

**$Na^+$ channel environment and composition—**The function of $Na^+$ channels (especially their late openings) is complex and not fully determined by their protein structure, but also greatly depends on interactions with multiple molecules of the channel environment, the function of which could be, in turn, also $Ca^{2+}$-dependent and greatly altered in HF. In addition to the pore-forming α subunit and its auxiliary β subunits, the multi- protein $Na^+$ channel complex includes components of cytoskeleton, regulatory kinases and phosphatases, trafficking proteins, and extracellular matrix proteins embedded into lipid bilayer plasma membrane (see reviews (1,25)). Subsarcolemmal actin-fodrin cytoskeleton is involved in modulation of the $Na_v1.5$ inactivation gating (44,47). Breakdown of actin-fodrin cytoskeleton integrity leads to the activation-inactivation uncoupling (22) similar to that reported here (Fig. 2 A, B vs. C, D). The fodrin breakdown that occurs in some hearts disease states featuring poor $Ca^{2+}$ handling, can be mediated by the $Ca^{2+}$/CaM via enzymes calpain and caspase (32,51). Accordingly, these **indirect** mechanisms can contribute to the CaM effect on SSI in failing myocytes reported here.

**Possible specific mechanisms for the differences—**While the greater modulation range for CaMKII in failing cells found in the present study is likely due to a higher expression of CaMKII in HF (see review (53)), the mechanism of CaM effect on SSI in failing hearts is not clear. As to $Na_v1.5$, it is still ambiguous if its SSI is (39) or is not (9,50,52) regulated by CaM. Our data in normal cardiomyocytes rather supports the latter hypothesis. Thus, possibilities for the specific $I_{NaL}$ regulation by CaM in HF include indirect effect of CaM (via molecules of the $Na^+$ channel complex, see above) or expression of other $Na^+$ channel isoforms modulated by CaM. Different transcripts of highly TTX-sensitive neuronal isoforms ($Na_v1.1$, 1.3, 1.6) have been indeed identified in mouse and dog heart ($Na_v1.1$, 1.2, 1.3) (12,15). These neuronal $Na^+$ channel isoforms are responsible for 10 to 20% of the $Na^+$ current peak in myocardial and Purkinje cells, respectively (12). CaM also shifts SSI curve for the skeletal muscle isoform $Na_v1.4$ (9,52). Furthermore, four splice variants of SCN5A gene that encodes $Na_v1.5$ have been reported in humans and they differ in their biophysical properties (38). Contributions of these variants and/or isoforms into cardiac $I_{NaL}$ and their modulation by different pathological conditions are not yet understood and need further studies.

### 4.3. Significance of $I_{NaL}$ modulation by $Ca^{2+}$ for normal heart function

$Ca^{2+}$ modulation of $I_{NaL}$ likely contributes to cell $Na^+/Ca^{2+}$ balance, which is critical for normal and enhanced cardiomyocyte performance. More specifically, $Ca^{2+}$ dependent increase of $I_{NaL}$ may provide a novel mechanism contributing to a well known Bowditch-Treppe effect postulating that an increase in the heart rate leads to an increase in the force of contraction (inotropic effect of rate). This fundamental law defines the net heart performance when demand for blood pumping increases. Higher cell $Ca^{2+}$ levels, which are required for stronger contractions, can be preserved with increased $Na^+$ influx via $I_{NaL}$ during AP plateau by the $Ca^{2+}$-dependent positive feedback mechanism discovered in the present study. The

contribution of this mechanism is thus linked to a higher cellular $Na^+$, which, in turn, decreases $Ca^{2+}$ extrusion by NCX.

### 4.4. Significance of $I_{NaL}$ and its modulation by $Ca^{2+}$ in heart failure

Chronic HF is characterized by both cardiac arrhythmias and reduced contractility, and $I_{NaL}$ likely contributes to these problems, as partial blockade of $I_{NaL}$ normalizes AP repolarization, inhibits EADs, and greatly improves contractility of failing VCs (16,21,46). $I_{NaL}$ decay is significantly slowed and $I_{NaL}$ density is increased in VCs of chronic human and canine HF (21,46). The importance of $I_{NaL}$ relative to other currents can be grater in HF, because $K^+$ current and $I_{NaT}$ are downregulated in failing myocardium (7,19,48,54). For example, after 500 ms of membrane depolarization $I_{NaL}$ becomes comparable with $I_{CaL}$ ($I_{NaL}$= 0.68*$I_{CaL}$) in canine failing VCs (46). Thus, $I_{NaL}$ greatly contributes to the ion current balance on the AP plateau (36,45) as well as to cell $Na^+$ influx (21), and thereby indirectly to cell $Ca^{2+}$ regulation via NCX ((17,42), review (5)).

The increased net $I_{NaL}$ provides additional $Na^+$ influx in failing cardiomyocytes by ~54 to 58% (21,23) and the total $I_{NaL}$-mediated $Na^+$ influx is almost equal to that mediated by $I_{NaT}$ (23). The rise of $I_{NaL}$-related $Na^+$ influx can explain, at least in part, the increased cell $Na^+$ load documented in HF (4,10,30). The $I_{NaL}$ contribution might be even larger, because $I_{NaL}$ was always measured at low $[Ca^{2+}]_i$ in the previous studies, but the present study identified strong positive $I_{NaL}$ modulation by $[Ca^{2+}]_i$ (Fig. 1,Table . The effect of $Ca^{2+}$ modulation was observed within the voltage range of AP plateau (Fig.2 B). Accordingly, the $Na^+$ overload, in turn, is expected to shift the operation of NCX (upregulated in HF (37)) during the AP plateau from the forward to the reverse mode of operation, leading to a higher cell $Ca^{2+}$ load.

This $Na^+$-driven higher $Ca^{2+}$ load limits depression of systolic function of failing VCs (5) and thus can be considered as an intrinsic, adaptive, digitalis-like effect with all corresponding risks and benefits. Interestingly, a large burst mode component of the $Na^+$ current has been identified in post-myocardial infarction-remodeled myocytes (13), i.e. in the transitional period from an infarction to HF. The increased $I_{NaL}$ may indeed serve as an initial adaptation mechanism to match an increased contractility demand for the survived VCs.

On the other hand, $Ca^{2+}$ overload has substantial adverse effects in failing hearts including: 1) arrhythmias via increased probability of spontaneous $Ca^{2+}$ release and DADs, and 2) failing contractility due to diastolic dysfunction, especially at high heart rates. In addition to the problems of $Ca^{2+}$ overload, the increased $I_{NaL}$ prolongs AP plateau and leads to beat-to-beat variability of AP duration, and EADs (16,21,42,46), which may also cause arrhythmias (40). Interestingly, decay kinetics of $I_{CaL}$ and $I_{NaL}$ are regulated in the opposite ways by $Ca^{2+}$, i.e. accelerating (2) and slowing (this study), respectively. As failing VCs are loaded with $Ca^{2+}$, the mechanism of the $Ca^{2+}$-induced-$I_{NaL}$ increase may thus provide a positive feedback mechanism to increase further $Na^+$ influx and facilitate cell $Ca^{2+}$ overload, thus exaggerating further the aforementioned HF-related problems.

### 4.5. $Ca^{2+}$ modulates gating modes of late $Na^+$ channel openings

We interpret our results in terms of channel gating based on previous single channel studies and numerical modeling of $I_{NaL}$ (see section 3.5). CaMKII is expected to slow inactivation kinetics of both burst mode and LSM (to a greater extent in HF) and to decrease the number of burst mode channels; $Ca^{2+}$ (independently on CaM) increases the number of LSM channels specifically in failing myocytes. The effect of $Ca^{2+}$ on bursts is in line with that the cytoskeleton integrity and lysophosphatidylcholine affect the burst mode of $Na^+$ channel openings (43,47). These modulators are $Ca^{2+}$-dependent: the cytoskeleton is affected by calpain and caspase (see section 4.1), and lysophosphatidylcholine is a substrate for protein kinase C (27). We found

that instant $Ca^{2+}$ modulation in failing cells is much greater at the beginning of depolarization (shaded area in Fig.7C), indicating that $Ca^{2+}$ regulates not only $Na^+$ total influx via $I_{NaL}$ but also complex $I_{NaL}$ dynamics, contributed by different gating modes of late channel openings. More specifically, while the integral of the burst mode (i.e. $Q_{BM}$) remains almost the same at various $[Ca^{2+}]_i$ (Table 4), the dynamic contribution of bursts into $I_{NaL}$ is greatly modulated by $[Ca^{2+}]_i$ in HF. Since bursts are active early after depolarization onset (45), this modulation, in turn, could be important for early repolarization phase (the "notch" phase), which is altered in HF (in our canine model and humans (16,46)) and determines the synchronicity of the $Ca^{2+}$ release (see review (35)), and thereby the quality of EC coupling.

### 4.6. Targeting $I_{NaL}$ is a novel approach in prevention of ventricular arrhythmia and diastolic dysfunction in HF

Based on the discovery that amiodarone effectively and selectively reduces $I_{NaL}$ compared to $I_{NaT}$ in human failing myocardium, we have previously suggested a new therapeutic strategy for cardioprotection by a selective inhibition of $I_{NaL}$ (20). Our most recent finding in failing VCs was that ranolazine blocks $I_{NaL}$ (41) even more selectively than amiodarone, and this new strategy of $I_{NaL}$ blockade is now seriously considered by clinical cardiologists in future therapies to prevent cardiac arrhythmias and $Ca^{2+}$ overload both in HF and cardiac ischemia (8). The results of the present study indicate that $I_{NaL}$ can be also targeted indirectly via $Ca^{2+}$ signaling. More specifically, as CaMKII was found to be upregulated in human HF (review (53)), $I_{NaL}$ decay can be potentially accelerated by a CaMKII inhibition as well as by intracellular $Ca^{2+}$ buffering, or by prevention of CaM binding.

## Study limitations

Although the 1 μM $[Ca^{2+}]_i$ used in the study is high (but still within a physiological range for VCs), its effect on $I_{NaL}$ can be exaggerated because of a prolong influence of $Ca^{2+}$ at the steady-state that is different from dynamic $Ca^{2+}$ variations in intact beating cells. Studies of the dynamic modulation of $I_{NaL}$ by $Ca^{2+}$ (including numerical modeling of AP in HF) as well as of detailed molecular mechanisms of the modulation merit further consideration. Although we suggest $I_{NaL}$ and its $Ca^{2+}$ regulation as potential targets for cardioprotection, this should be considered with caution as $I_{NaL}$ inhibition can decrease systolic function and in some cases can be pro-arrhythmic, when the $I_{NaL}$-mediated AP prolongation is associated with an anti-reentry effect.

#### Acknowledgements

**Grants** This study was supported by grants from the National Heart, Lung and Blood Institute HL-53819, HL074238 (A Undrovinas), and by a grant-in-aid from the American Heart Association 0350472Z (A Undrovinas).

## References

1. Abriel H, Kass RS. Regulation of the voltage-gated cardiac sodium channel Nav1.5 by interacting proteins. Trends Cardiovasc Med 2005;15:35–40. [PubMed: 15795161]
2. Alseikhan BA, DeMaria CD, Colecraft HM, Yue DT. Engineered calmodulins reveal the unexpected eminence of $Ca^{2+}$ channel inactivation in controlling heart excitation. Proc Natl Acad Sci U S A 2002;99:17185–90. [PubMed: 12486220]
3. Aman TK, Raman IM. Subunit dependence of Na channel open-channel block and slow inactivation in cerebellar neurons. Biophys J 2006;22:22.
4. Baartscheer A, Schumacher CA, Belterman CN, Coronel R, Fiolet JW. $[Na^+]$i and the driving force of the $Na^+/Ca^{2+}$ -exchanger in heart failure. Cardiovasc Res 2003;57:986–95. [PubMed: 12650876]
5. Bers DM. Altered cardiac myocyte Ca regulation in heart failure. Physiology (Bethesda) 2006;21:380–7. [PubMed: 17119150]

6. Bers DM, Despa S. Cardiac myocytes $Ca^{2+}$ and $Na^{+}$ regulation in normal and failing hearts. J Pharmacol Sci 2006;100:315–22. [PubMed: 16552170]
7. Beuckelmann DJ, Nabauer M, Erdmann E. Alterations of $K^{+}$ currents in isolated human ventricular myocytes from patients with terminal heart failure. Circ Res 1993;73:379–85. [PubMed: 8330380]
8. Conti CR. Inhibition of sodium-dependent calcium overload to treat myocardial ischemia. Clin Cardiol 2006;29:141–3. [PubMed: 16649721]
9. Deschenes I, Neyroud N, DiSilvestre D, Marban E, Yue DT, Tomaselli GF. Isoform-specific modulation of voltage-gated $Na^{+}$ channels by calmodulin. Circ Res 2002;90:E49–57. [PubMed: 11884381]
10. Despa S, Islam MA, Weber CR, Pogwizd SM, Bers DM. Intracellular $Na^{+}$ concentration is elevated in heart failure but Na/K pump function is unchanged. Circulation 2002;105:2543–8. [PubMed: 12034663]
11. Dumaine R, Wang Q, Keating MT, Hartmann HA, Schwartz PJ, Brown AM, Kirsch GE. Multiple mechanisms of $Na^{+}$ channel--linked long-QT syndrome. Circ Res 1996;78:916–24. [PubMed: 8620612]
12. Haufe V, Cordeiro JM, Zimmer T, Wu YS, Schiccitano S, Benndorf K, Dumaine R. Contribution of neuronal sodium channels to the cardiac fast sodium current $I_{Na}$ is greater in dog heart Purkinje fibers than in ventricles. Cardiovasc Res 2005;65:117–27. [PubMed: 15621039]
13. Huang B, El-Sherif T, Gidh-Jain M, Qin D, El-Sherif N. Alterations of sodium channel kinetics and gene expression in the postinfarction remodeled myocardium. J Cardiovasc Electrophysiol 2001;12:218–25. [PubMed: 11232622]
14. Kameyama M, Hofmann F, Trautwein W. On the mechanism of beta-adrenergic regulation of the Ca channel in the guinea-pig heart. Pflugers Arch 1985;405:285–93. [PubMed: 2415919]
15. Maier S, Westenbroek R, Yu FH, Vien T, Scheuer T, Catterall WA. Functional expression and localization of brain $Na_v1.1$ sodium channel α-subunits in single cardiac myocytes. Circulation 2001;104:II–309.
16. Maltsev VA, Sabbah HN, Higgins RSD, Silverman N, Lesch M, Undrovinas AI. Novel, ultraslow inactivating sodium current in human ventricular cardiomyocytes. Circulation 1998;98:2545–2552. [PubMed: 9843461]
17. Maltsev VA, Sabbah HN, Tanimura M, Lesch M, Goldstein S, Undrovinas AI. Relationship between action potential, contraction-relaxation pattern, and intracellular $Ca^{2+}$ transient in cardiomyocytes of dogs with chronic heart failure. Cell Molec Life Sci 1998;54:597–605. [PubMed: 9676578]
18. Maltsev VA, Sabbah HN, Undrovinas AI. Calmodulin modulates late sodium current in normal and failing myocardium. Circulation 2002;106:II–227.
19. Maltsev VA, Sabbah HN, Undrovinas AI. Down-regulation of sodium current in chronic heart failure: effects of long-term therapy with carvedilol. Cell Mol Life Sci 2002;59:1561–8. [PubMed: 12440776]
20. Maltsev VA, Sabbah HN, Undrovinas AI. Late sodium current is a novel target for amiodarone: Studies in failing human myocardium. J Mol Cell Cardiol 2001;33:923–932. [PubMed: 11343415]
21. Maltsev VA, Silverman N, Sabbah HN, Undrovinas AI. Chronic heart failure slows late sodium current in human and canine ventricular myocytes: Implications for repolarization variability. Eur J Heart Fail 2007;9:219–227. [PubMed: 17067855]
22. Maltsev VA, Undrovinas AI. Cytoskeleton modulates coupling between availability and activation of cardiac sodium channel. Am J Physiol Heart Circ Physiol 1997;27342:H1832–H1840. [PubMed: 9362250]
23. Maltsev VA, Undrovinas AI. A multi-modal composition of the late $Na^{+}$ current in human ventricular cardiomyocytes. Cardiovasc Res 2006;69:116–127. [PubMed: 16223473]
24. Mathias RT, Cohen IS, Oliva C. Limitations of the whole cell patch clamp technique in the control of intracellular concentrations. Biophys J 1990;58:759–70. [PubMed: 2169920]
25. Meadows LS, Isom LL. Sodium channels as macromolecular complexes: implications for inherited arrhythmia syndromes. Cardiovasc Res 2005;67:448–58. [PubMed: 15919069]
26. Noble D, Noble PJ. Late sodium current in the pathophysiology of cardiovascular disease: consequences of sodium-calcium overload. Heart 2006;92:iv1–iv5. [PubMed: 16775091]

27. Obata T. Adenosine production and its interaction with protection of ischemic and reperfusion injury of the myocardium. Life Sci 2002;71:2083–103. [PubMed: 12204768]
28. Oliva C, Cohen IS, Mathias RT. Calculation of time constants for intracellular diffusion in whole cell patch clamp configuration. Biophys J 1988;54:791–9. [PubMed: 3242629]
29. Patlak JB, Ortiz M. Slow currents through single sodium channels of the adult rat heart. J Gen Physiol 1985;86:89–104. [PubMed: 2411848]
30. Pieske B, Maier LS, Piacentino V 3rd, Weisser J, Hasenfuss G, Houser S. Rate dependence of [$Na^+$]i and contractility in nonfailing and failing human myocardium. Circulation 2002;106:447–53. [PubMed: 12135944]
31. Pusch M, Neher E. Rates of diffusional exchange between small cells and a measuring patch pipette. Pflugers Arch 1988;411:204–11. [PubMed: 2451806]
32. Rotter B, Kroviarski Y, Nicolas G, Dhermy D, Lecomte MC. AlphaII-spectrin is an in vitro target for caspase-2, and its cleavage is regulated by calmodulin binding. Biochem J 2004;378:161–8. [PubMed: 14599290]
33. Sabbah HN, Goldberg AD, Schoels W, Kono T, Webb C, Brachmann J, Goldstein S. Spontaneous and inducible ventricular arrhythmias in a canine model of chronic heart failure: relation to haemodynamics and sympathoadrenergic activation. Eur Heart J 1992;13:1562–72. [PubMed: 1281453]
34. Sabbah HN, Stein PD, Kono T, Gheorghiade M, Levine TB, Jafri S, Hawkins ET, Goldstein S. A canine model of chronic heart failure produced by multiple sequential coronary microembolizations. Am J Physiol 1991;260:H1379–84. [PubMed: 1826414]
35. Sah R, Ramirez RJ, Oudit GY, Gidrewicz D, Trivieri MG, Zobel C, Backx PH. Regulation of cardiac excitation-contraction coupling by action potential repolarization: role of the transient outward potassium current (I(to)). J Physiol 2003;546:5–18. [PubMed: 12509475]
36. Sakmann BF, Spindler AJ, Bryant SM, Linz KW, Noble D. Distribution of a persistent sodium current across the ventricular wall in guinea pigs. Circ Res 2000;87:910–4. [PubMed: 11073887]
37. Studer R, Reinecke H, Bilger J, Eschenhagen T, Bohm M, Hasenfuss G, Just H, Holtz J, Drexler H. Gene expression of the cardiac $Na^+$ -$Ca^{2+}$ exchanger in end-stage human heart failure. Circ Res 1994;75:443–53. [PubMed: 8062418]
38. Tan BH, Valdivia CR, Rok BA, Ruwaldt KM, Tester DJ, Ackerman MJ, Makielski JC. Common human SCN5A polymorphisms have altered electrophysiology when expressed in Q1077 splice variants. Heart Rhythm 2005;2:741–747. [PubMed: 15992732]
39. Tan HL, Kupershmidt S, Zhang R, Stepanovic S, Roden DM, Wilde AA, Anderson ME, Balser JR. A calcium sensor in the sodium channel modulates cardiac excitability. Nature 2002;415:442–447. [PubMed: 11807557]
40. Tomaselli GF, Zipes DP. What causes sudden death in heart failure? Circ Res 2004;95:754–763. [PubMed: 15486322]
41. Undrovinas AI, Belardinelli L, Undrovinas NA, Sabbah HN. Ranolazine improves abnormal repolarization and contraction in left ventricular myocytes of dog with heart failure by inhibiting late sodium current. J Cardiovasc Electrophys 2006;17:S1–S9.
42. Undrovinas AI, Belardinelli L, Undrovinas NA, Sabbah HN. Ranolazine improves abnormal repolarization and contraction in left ventricular myocytes of dogs with heart failure by inhibiting late sodium current. J Cardiovasc Electrophysiol 2006;17:S169–S177. [PubMed: 16686675]
43. Undrovinas AI, Fleidervish IA, Makielski JC. Inward sodium current at resting potentials in single cardiac myocytes induced by the ischemic metabolite lysophosphatidylcholine. Circ Res 1992;71:1231–41. [PubMed: 1327577]
44. Undrovinas AI, Maltsev VA. Spectrin-based cytoskeleton modulates late sodium currents in heart. Biophys J 2003;84:25A.
45. Undrovinas AI, Maltsev VA, Kyle JW, Silverman NA, Sabbah HN. Gating of the late $Na^+$ channel in normal and failing human myocardium. J Mol Cell Cardiol 2002;34:1477–1489. [PubMed: 12431447]
46. Undrovinas AI, Maltsev VA, Sabbah HN. Repolarization abnormalities in cardiomyocytes of dogs with chronic heart failure: Role of sustained inward current. Cell Mol Life Sci 1999;55:494–505. [PubMed: 10228563]

47. Undrovinas AI, Shander GS, Makielski JC. Cytoskeleton modulates gating of voltage-dependent sodium channel in heart. American Journal of Physiology 1995;269:H203–14. [PubMed: 7631850]

48. Valdivia CR, Chu WW, Pu J, Foell JD, Haworth RA, Wolff MR, Kamp TJ, Makielski JC. Increased late sodium current in myocytes from a canine heart failure model and from failing human heart. J Mol Cell Cardiol 2005;38:475–83. [PubMed: 15733907]

49. Wagner S, Dybkova N, Rasenack EC, Jacobshagen C, Fabritz L, Kirchhof P, Maier SK, Zhang T, Hasenfuss G, Brown JH, Bers DM, Maier LS. Ca/calmodulin-dependent protein kinase II regulates cardiac Na channels. J Clin Invest 2006;22:22.

50. Wingo TL, Shah VN, Anderson ME, Lybrand TP, Chazin WJ, Balser JR. An EF-hand in the sodium channel couples intracellular calcium to cardiac excitability. Nat Struct Mol Biol 2004;11:219–25. [PubMed: 14981509]

51. Yoshida K, Inui M, Harada K, Saido TC, Sorimachi Y, Ishihara T, Kawashima S, Sobue K. Reperfusion of rat heart after brief ischemia induces proteolysis of calspectin (nonerythroid spectrin or fodrin) by calpain. Circ Res 1995;77:603–10. [PubMed: 7641330]

52. Young KA, Caldwell JH. Modulation of skeletal and cardiac voltage-gated sodium channels by calmodulin. J Physiol 2005;565:349–70. [PubMed: 15746172]

53. Zhang T, Brown JH. Role of Ca2+/calmodulin-dependent protein kinase II in cardiac hypertrophy and heart failure. Cardiovasc Res 2004;63:476–86. [PubMed: 15276473]

54. Zicha S, Maltsev VA, Nattel S, Sabbah HN, Undrovinas AI. Post-transcriptional alterations in the expression of cardiac $Na^+$ channel subunits in chronic heart failure. J Mol Cell Cardiol 2004;37:91–100. [PubMed: 15242739]

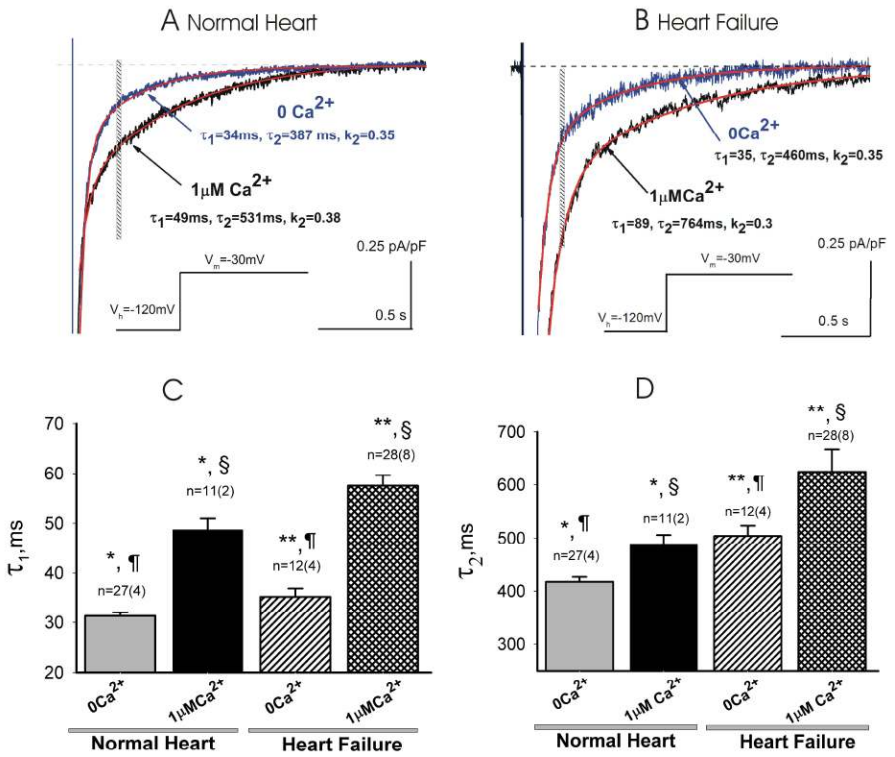


**Fig. 1.**

$Ca^{2+}$ modulates $I_{NaL}$ kinetics and amplitude in ventricular cardiomyocytes of normal and failing dog hearts. Representative raw traces were recorded at different $[Ca^{2+}]_i$ in normal (A) and failing (B) cells. Exponential fits (Eq.1, see Methods) are shown by solid lines together with their parameters. Inset shows voltage-clamp protocol. Vertical bars indicate (here and in other figures) the time window (200-220 ms of depolarization) used to evaluate $I_{NaL}$ density. Statistical data for the decay time constants $\tau_1$ (C) and $\tau_2$ (D), as well as $I_{NaL}$ density (E) at different $[Ca^{2+}]_i$ in normal and failing hearts. Bars represent average data mean ± SEM, N=number of cells (hearts). Statistical significant difference (P<0.05, ANOVA followed by Bonferroni's post hock test): *,** Normal and failing heart $0Ca^{2+}$ vs. $1\mu MCa^{2+}$, respectively, $^{\&,\prime}$ Normal *vs*. failing heart at $0Ca^{2+}$ and. $1\mu MCa^{2+}$, respectively.

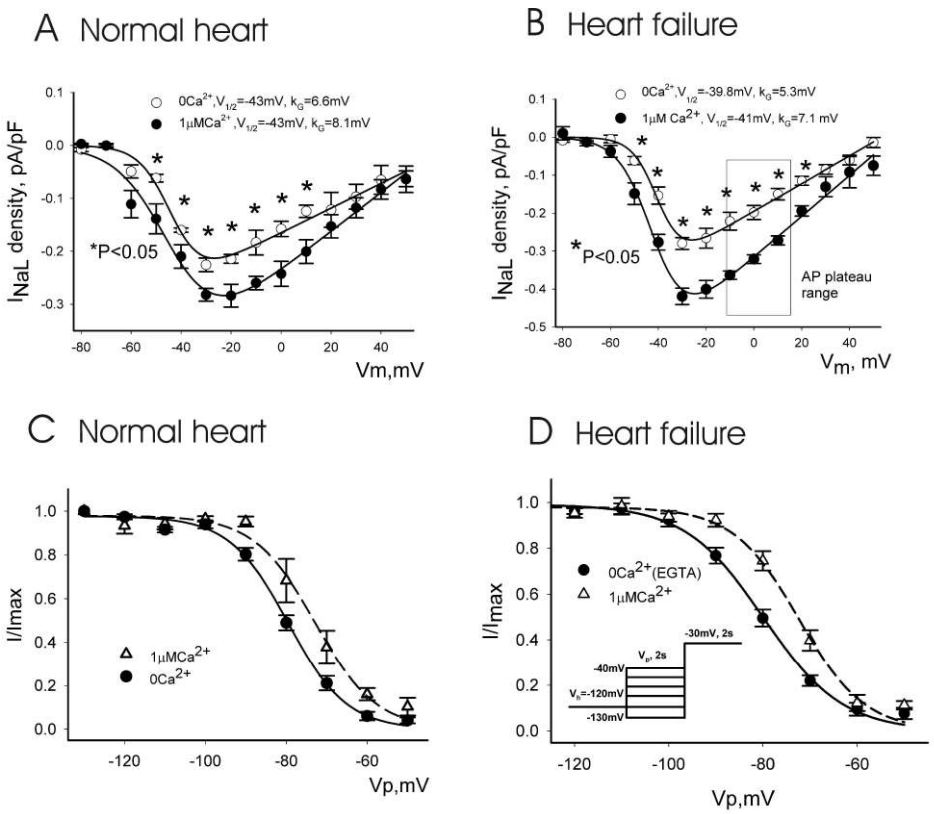


**Fig.2.**

Elevation of the intracellular $Ca^{2+}$ from 0 to 1μM uncouples the steady-state activation (SSA) and inactivation (SSI) of $I_{NaL}$ in both normal and failing hearts. (A,B), $I_{NaL}$-voltage relationship at different $[Ca^{2+}]_i$ ) in normal and failing hearts, respectively. Data represent mean ± SEM pooled from 4-11 cells. The solid lines show theoretical curves of SSA (Eq.3, Methods) fitted to data points. Maximum $I_{NaL}$ conductance $G_{max}$ significantly increased from 2.34 to 3.68 pS/pF (normal hearts) and from 3.65 to 5.38 pS/pF (HF) ($P<0.001$, F-test). Other fit parameters ($V_{1/2}$ and k are shown at the traces) remained almost unchanged in augmented $[Ca^{2+}]_i$. ). Action potential (AP) plateau range from −15 to 20 mV (46) is depicted by a box (B). SSI was significantly shifted rightward in response to the elevated $[Ca^{2+}]_i$ in both normal (C) and failing (D) hearts ($P<0.001$, F-test). Solid lines represent theoretical curve fit (Eq. 2, Methods). Statistical comparison of all SSI parameters for experiments is given in the text. Data points were pooled from the 5-20 cells (3 normal and 6 HF dogs). Inset in D shows voltage-clamp protocol.

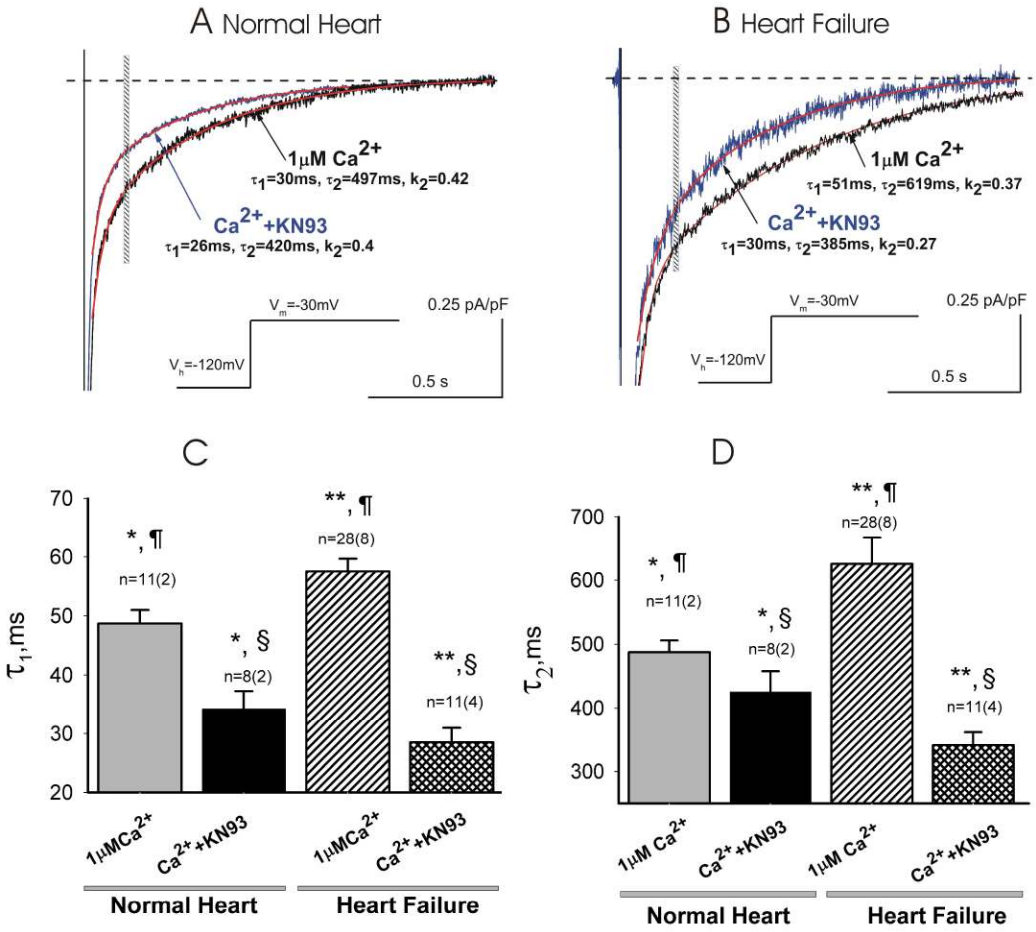


**Fig.3.**

Inhibition of CaMKII accelerates $I_{NaL}$ decay in normal and failing hearts. Representative raw traces were recorded at high $[Ca^{2+}]_i$ alone or in the presence of CaMKII inhibitor KN93 (10μM) in normal (A) and failing (B) cells. Exponential fits (Eq.1, see Methods) are shown by solid lines together with their parameters. Inset shows voltage-clamp protocol. C, D - Statistical data for the decay time constants $\tau_1$ and $\tau_2$ in normal and failing hearts, respectively. Bars represent average data mean ± SEM, N=number of cells (hearts). For decay time constants (C, D) statistical significant difference ($P<0.05$, ANOVA followed by Bonferroni's post hock test): *,** Normal and failing heart 1μM$Ca^{2+}$ vs. 1μM$Ca^{2+}$+KN93, respectively. & Normal vs. Failing heart at 1μM$Ca^{2+}$.

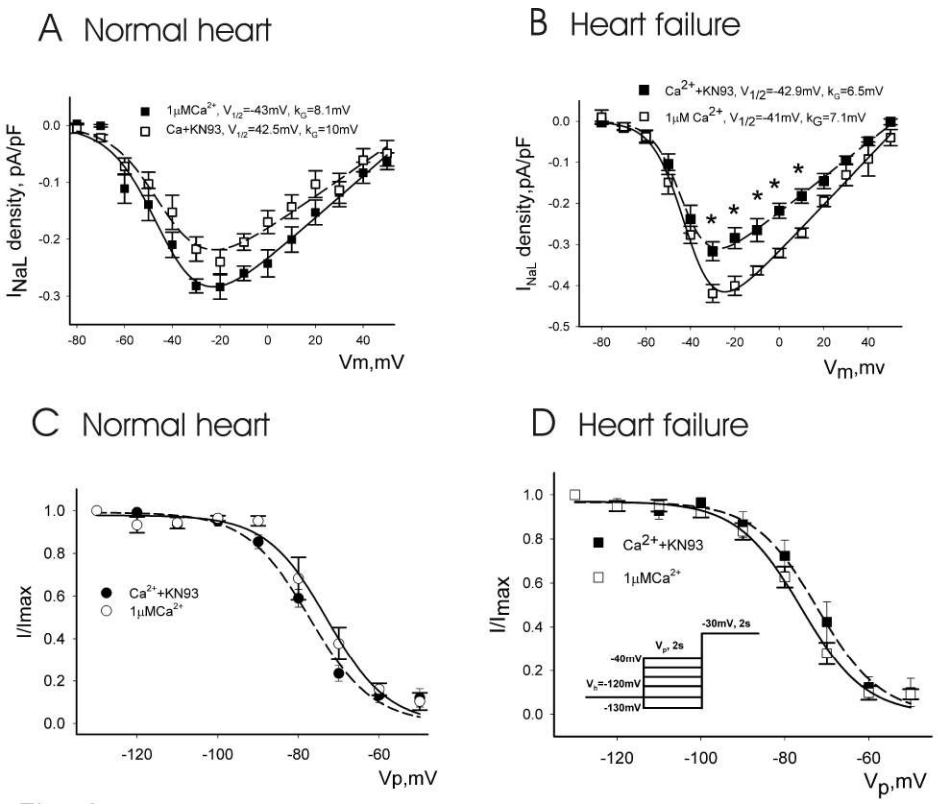


**Fig. 4.**

Effects of CaMKII inhibition on SSA and SSI of $I_{NaL}$ in both normal and failing hearts. (A,B) $I_{NaL}$-voltage relationship at high $[Ca^{2+}]_i$ ) and in the presence on CaMKII inhibitor KN93 (10 μM) in normal (A) and failing (B) cells, respectively. Data represent mean ± SEM pooled from 4-5 cells (2 normal and 2 failing hearts). The solid lines show theoretical curves of SSA (Eq. 3, Methods) fitted to data points. In response to CaMKII inhibition maximum $I_{NaL}$ conductance $G_{max}$ does not significantly changed 3.7 vs. 4.0 pS/pF in normal hearts (A), but significantly reduced from 5.4 to 4.62 pS/pF in HF (B) ($P<0.05$, F-test). Other fit parameters ($V_{1/2}$ and k) are shown at the traces. SSI was not affected by the CaMKII inhibition in either normal (C) or failing hearts (D). Detailed statistical comparison of all SSI parameters for large number of experiments is given in the text (Table 3). Asterisks in D shows statistically significant ($P<0.05$) differences in data points. Data points were pooled from the 5-10 cells (2 normal and 3 HF dogs). Inset in D shows voltage-clamp protocol.

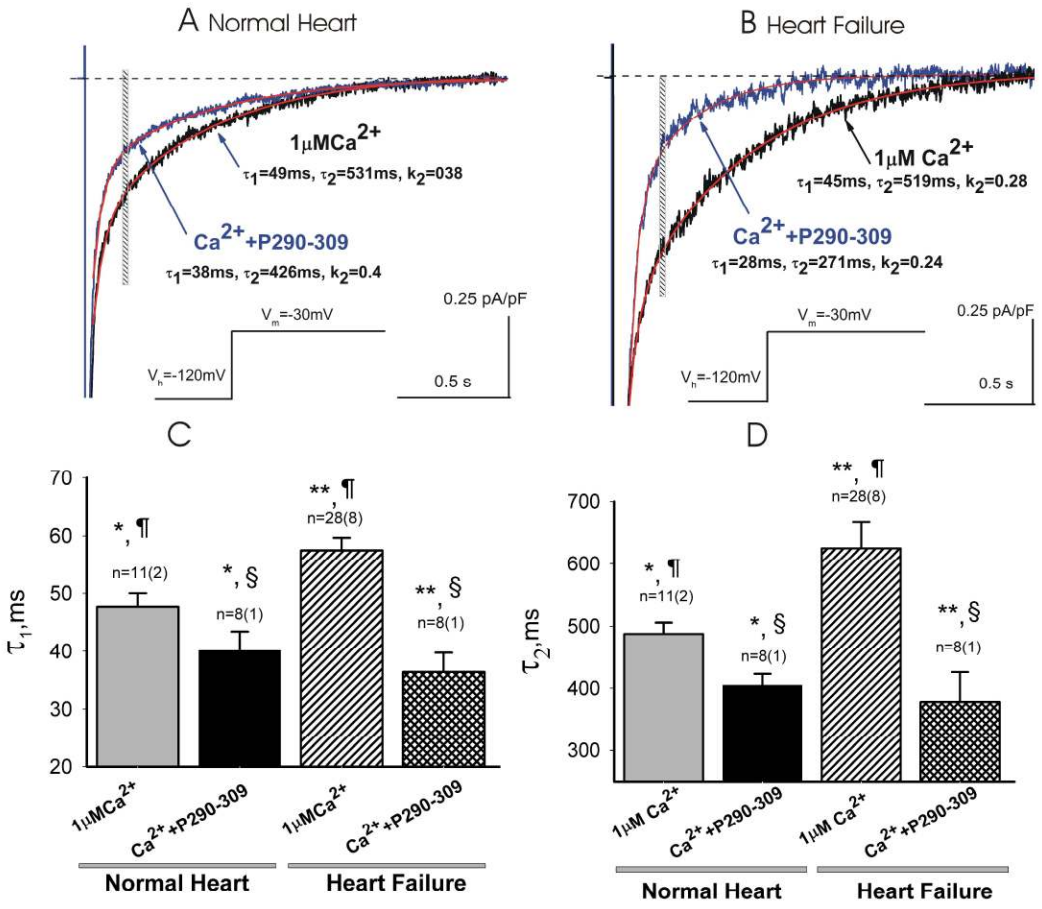


**Fig.5.**

Peptide P290-309 antagonist of $Ca^{2+}$-dependent CaM binding accelerates $I_{NaL}$ decay, and reduces its amplitude in normal and failing hearts. Representative raw traces were recorded at high $[Ca^{2+}]_i$ alone or in the presence of P290-309 in normal (A) and failing (B) cells. Exponential fits (Eq.1, see Methods) are shown by solid lines together with their parameters. Inset shows voltage-clamp protocol. Statistical data for the decay time constants $\tau_1$ (C) and $\tau_2$ (D) at different $[Ca^{2+}]_i$ in normal and failing hearts. Bars represent average data mean ± SEM, N=number of cells (hearts). Statistical significant difference ($P<0.05$, ANOVA followed by Bonferroni's post hock test): *,** Normal and failing heart $1\mu MCa^{2+}$ vs. $1\mu MCa^{2+}$+P290-309, respectively. & Normal vs. Failing heart at $1\mu MCa^{2+}$ (C, D). No significant difference: `Normal vs. failing heart at $1\mu MCa^{2+}$+P290-309 (C, D)

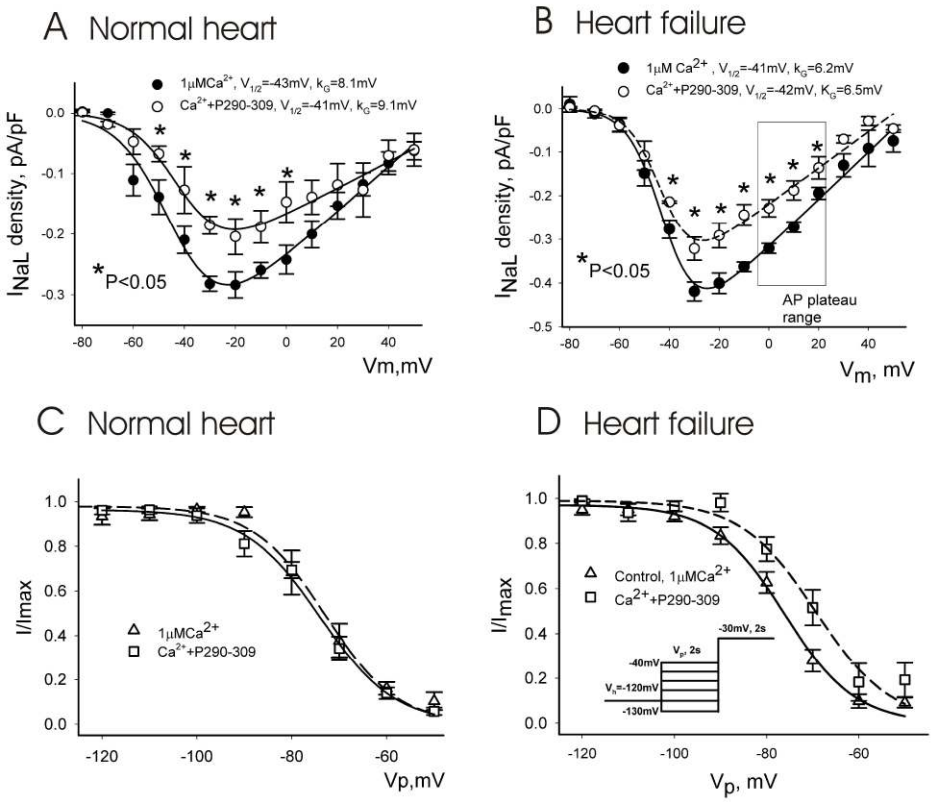


**Fig.6.**

Effects of blockade of $Ca^{2+}$- dependent CaM binding by the peptide P290-309 on the steady-state activation (SSA) and inactivation (SSI) of $I_{NaL}$ in both normal and failing hearts. (A, B) $I_{NaL}$-voltage relationship at high $[Ca^{2+}]_i$ ) alone or in the presence of P290-309 in normal and failing hearts, respectively. Data represent mean ± SEM pooled from 4-10 cells (2 normal and 2 failing hearts). The solid lines show theoretical curves of SSA (Eq.3, Methods) fitted to data points. Maximum $I_{NaL}$ conductance $G_{max}$ significantly decreased 3.68 to 2.17 pS/pF (normal hearts) and from 5.38 to 4.12 pS/pF (HF) ($P<0.001$, F-test) in the presence of P290-309. Other fit parameters ($V_{1/2}$ and k are shown at the traces) remained almost unchanged in augmented $[Ca^{2+}]_i$). Action potential (AP) plateau range from −15 to 20 mV (46) is depicted by a box (B). The theoretical curve of SSI was significantly shifted rightward in the presence of P290-309 in HF (D, $P<0.001$ F-test), but not in normal (C) hearts. Statistical comparison of all SSI parameters for experiments is given in the text. Data points were pooled from the 5-20 cells (3 normal and 6 HF dogs). Inset in D shows voltage-clamp protocol.

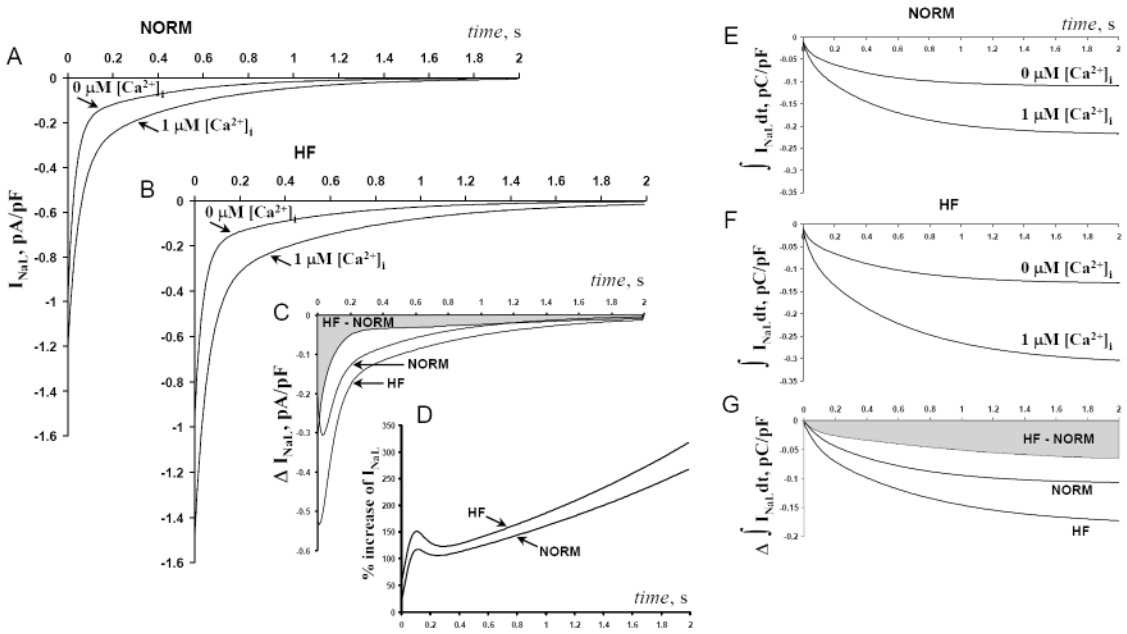


**Fig. 7.**

Theoretical evaluation of difference in the cumulative effects of the elevated $Ca^{2+}$ on $I_{NaL}$ and its integral (~ $Na^+$ influx) in cardiomyocytes of normal dogs (NORM) and dogs with chronic heart failure (HF). Parameters for idealized, two-exponential $I_{NaL}$ decay time course were assigned from the average experimental data measured in two extreme conditions: $[Ca^{2+}]_i$=0, and $[Ca^{2+}]_i$=1 μM (see section 3.5 for details). The average maximum $I_{NaL}$ density at -30 mV was corrected for SSI voltage-dependence assuming a resting/holding potential of -80 mV. A and B, idealized $I_{NaL}$ in normal and failing ventricular myocytes, respectively. C and D, the absolute and relative ranges of $Ca^{2+}$ regulation of $I_{NaL}$ are larger in failing cells (the absolute difference is shown by shaded area in C). E and F: substantial modulation of $I_{NaL}$-related $Na^+$ influx by $Ca^{2+}$ assessed as an absolute value of $I_{NaL}$ integral in normal and failing myocytes. G: the modulation of $I_{NaL}$-related $Na^+$ influx by $Ca^{2+}$ is greater in failing myocytes (shaded area "HF-NORM").

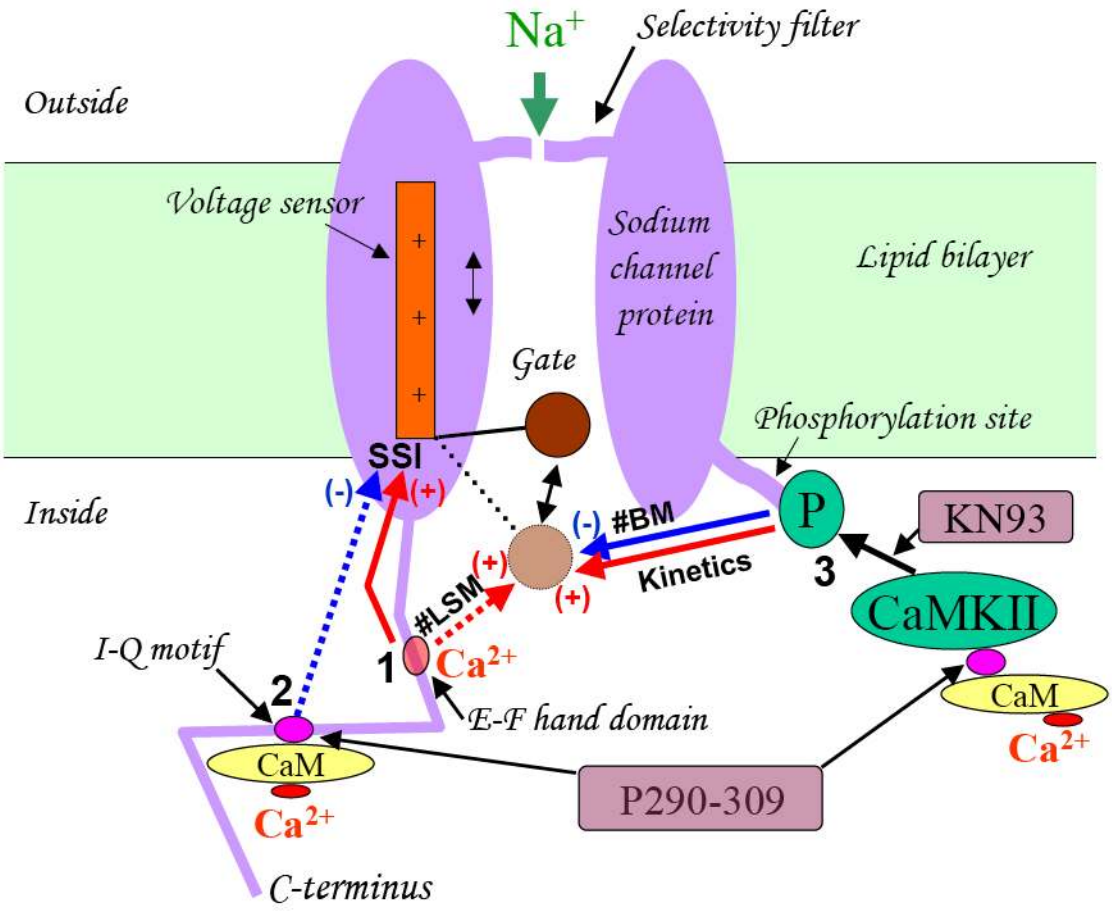


**Figure 8.**

Simplified hypothetical diagram of the intracellular $Ca^{2+}$ signaling pathways modulating late sodium current in normal and failing canine ventricular myocytes based on the results of the present study. Pathways 1, 2 and 3 (marked by black digits) represent $Ca^{2+}$ binding to: the E-F domain, CaM-binding site (IQ motif) on C-terminus of Na channel (NaCh) as well as CaM/CaMKII complex, respectively. Arrows with plus/minus signs indicate modulation in terms of increase/decrease of $I_{NaL}$ integral. Biophysical mechanisms of the the modulations are shown as follows: SSI, the shift of the voltage dependency of steady-state inactivation. #LSM and #BM, the number of channels in late scattered or burst mode, respectively. Gating kinetics, slowing inactivation gating for LSM and BM. Please note that pathways shown by dashed lines are effective only in failing myocytes. Also shown are the inhibitory sites of the CaM antagonist peptide P290-309 and KN93 - inhibitor of CaMKII employed in the present study to test the signaling.

**Table 1**

Composition of bath (B) and pipette (P) solutions used in the study. Abbreviations: TEA- tetraethylammonium, EGTA- ethylene glycolbis(beta-amonoethyl ether)N,N,N',N'-tertraacetic acid, HEPES-N-[2-hydroxyethyl] piperazine-N'- [2ethanesulfonic acid], BAPTA-Ethylenedioxybis(o-phenylenenitrilo)tetraacetic acid.

| | **Pipette solution, mM** | | | **Bath solution, mM** |
|---|---|---|---|---|
| | **P1 (0 $Ca^{2+}$, EGTA)** | **P2 (0 $Ca^{2+}$, BAPTA)** | **P3 (1μM $Ca^{2+}$)** | **B** |
| NaCl | 5 | 5 | 5 | 140 |
| CsCl | 133 | 133 | 133 | 5.4 |
| $CaCl_2$ | | | 0.9 | 1.8 |
| $MgCl_2$ | | | | 2 |
| MgATP | 2 | 2 | 2 | |
| TEA | 20 | 20 | 20 | |
| Nifedipine | | | | 0.002 |
| EGTA | 10 | | 1 | |
| BAPTA | | 10 | | |
| HEPES | 5 | 5 | 5 | 5 |
| pH | 7.3 | 7.3 | 7.3 | 7.3 |
| | CsOH | CsOH | CsOH | NaOH |

**Table 2**

Effects of intracellular $Ca^{2+}$ signaling on the density of $I_{NaL}$ in failing dog cardiomyocytes. The amplitude of $I_{NaL}$ was determined as an averaged current density within 200-220 ms after the onset of a 2 second long depolarization step at −30mV.

| Intracellular conditions | $I_{NaL}$ density, pA/pF | | N, cells (dogs) | |
|---|---|---|---|---|
| | HF | NH | HF | NH |
| 0 $Ca^{2+}$ | 0.31 ± 0.02 | 0.24 ± 0.01 | 26(5) | 37(5) |
| 1 μM $Ca^{2+}$ | 0.49 ± 0.03* | 0.34±0.03* | 12(3) | 13(2) |
| 1 μM$Ca^{2+}$+KN93 (10 μM) | 0.37 ± 0.03** | 0.26± 0.025 | 9(4) | 11(2) |
| 1 μM $Ca^{2+}$+P290-309 (10 μM) | 0.36 ± 0.01† | 0.25 ± .02† | 9(4) | 6(1) |

Data are mean ± SEM, (N)- first number is number of cells and the second number is the number of dogs. Statistical significant difference (P<0.05, ANOVA followed by Bonferroni's post hock test): * Normal and failing heart vs. 0$Ca^{2+}$; **,† Normal and failing heart vs. 1 μM $Ca^{2+}$; Normal vs. HF significant difference compared at the same conditions (not indicated).

**Table 3**

Effects of intracellular $Ca^{2+}$ signaling pathways on the steady-state inactivation parameters in normal and failing dog cardiomyocytes. Steady state inactivation of $I_{NaL}$ was assessed by a double pulse protocol, and was fitted to Boltzmann model (Equation 2, Methods) with mid-potential $V_{1/2}$ and slope $K_A$.

| Intracellular conditions | $V_{1/2}$, mV | | $K_A$, mV | | N, cells (dogs) | |
|---|---|---|---|---|---|---|
| | HF | NH | HF | NH | HF | NH |
| 0 $Ca^{2+}$ | -81.3 ± 3.9 | −80.1 ± 0.7 | -5.6 ± 0.4 | -6.3 ± 0.3 | 14 (3) | 38(5) |
| 1 μM $Ca^{2+}$ | -75.7 ± 3.7* | -73.9±1.9* | -7.2 ± 0.4* | -6.2 ± 0.8 | 15(4) | 6(2) |
| 1 μM $Ca^{2+}$+KN93 (10 μM) | -74.6 ± 1.5 | -77.9±1.6 | -5.2 ± 0.4 | -5.8 ± 0.9 | (7,3) | 7(2) |
| 1 μM $Ca^{2+}$+P290-309 (10 μM) | -70.2 ± 1.5** | -73.3±1.2 | -5.4 ± 0.5 | -5.4 ± 0.8 | (7,2) | 6(1) |

Data are mean ± SEM, N- first and second numbers are number of cells and dogs, respectively. Statistical comparison for $V_{1/2}$: *significantly different from 0 $Ca^{2+}$; ** significantly different from 1 μM $Ca^{2+}$ and 1μM$Ca^{2+}$ + KN93. For K: *significantly different from 0$Ca^{2+}$ (ANOVA followed by Bonferroni's post-hoc test). Differences were considered statistically significant for $P<0.05$. Abbreviations: NH-normal heart, HF-heart failure

**Table 4**

Results of numerical evaluation and comparison of different $Ca^{2+}$ -dependent mechanisms of $I_{NaL}$ modulation in normal and failing cardiomyocytes. The components describing $I_{NaL}$ fine structure and $I_{NaL}$ integrals presented in the table are described in section 3.5. Shaded cells indicate regulation components, which are substantially different in normal and failing cells. Each numerical estimate is accompanied by plus or minus signs reflecting semi-quantitively the strength of the change (just for guidance). NS denotes not significant change. Abbreviations for pipette solution: 0Ca, [$Ca^{2+}$]=0; 1Ca, [Ca2+]=1μM; P, Peptide 290-309; KN, KN93. $Q_{tot}$ was calculated (Eq. 8, section 3.5) at a physiological resting potential $V_h$=-80mV, and thus includes effects of corresponding SSI shifts. All other parameters, including $Q_{BM}$ and $Q_{LSM}$ (Eqs. 6,7, section 3.5), were calculated at $V_h$=-130mV. Values of the integrals are given in pC/pF.

| Modulatory mechanism | Component | Normal | | | Heart failure | | |
|---|---|---|---|---|---|---|---|
| | | Parameter change | Effect on the respective Integral | | Parameter change | Effect on the respective Integral | |
| Overall $Ca^{2+}$ dependence | All components | See Fig.7A | (+++) $Q_{tot}$: 0.103 (0Ca) to 0.211 (1Ca) by 101% | | See Fig.7B | (++++) $Q_{tot}$: 0.126 (0Ca) to 0.297 (1Ca) by 135% | |
| CaMKII | $I_{LSM}(0)$, pA/pF | (NS) 0.407 to 0.483 | (++) $Q_{LSM}$: 0.172 to 0.232 by 35% | (++) $Q_{tot}$: 0.141 (1Ca&KN) to 0.211 (1Ca) by 49.6% | NS 0.677 to 0.603 | (++) $Q_{LSM}$: 0.231 to 0.361 by 56.8%. | (+) $Q_{tot}$: 0.246 (1Ca&KN) to 0.297 (1Ca) by 20.7% |
| | $\tau_2$, ms | (+) 425 to 487 by 14.6% | | | (+++) 341 to 625 by 83.3% | | |
| | $I_{BM}(0)$ , pA/pF | (-) 1.94 to 1.19 | (NS) $Q_{BM}$: 0.0675 to 0.0584 | | (-) 3.53 to 1.70 | (NS) $Q_{BM}$: 0.102 to 0.099 | |
| | $\tau_1$, ms | (+) 34.3 to 48.6 by 41.7% | | | (+++) 28.5 to 57.5 By 202% | | |
| CaM | SSI shift, mV | No shift | (NS) | | (-) -5.3 mV -70.2 to -75.5 | (-) $Q_{tot}$: 0.246 (1Ca&KN) to 0.317 (1Ca&P) by 28.8% | |
| $Ca^{2+}$ (CaM independent) | $I_{LSM}(0)$, PA/pF | (NS) 0.383 to 0.394 | (++) $Q_{tot}$: increase 0.105 (0Ca) to 0.169 (1Ca&P) by 61.6% | | (++) 0.452 to 0.591 by 30.7% | (++++) $Q_{tot}$: 0.126 to 0.317 (1Ca&P) by 150% | |
| | SSI shift, mV | (+) +6.8 mV: -80.1 to -73.3 | | | (++) +11.1 mV: -81.3 to -70.2 | | |